DOI: 10.1002/ ((please add manuscript number))
Article type: Full Paper

Rapid and Repeatable Self-Healing Superoleophobic Porous Aluminum Surface Using Infiltrated Liquid Healing Agent

*Katsutoshi Nakayama, Akira Koyama, Chunyu Zhu, Yoshitaka Aoki, Hiroki Habazaki**

Dr. Katsutoshi Nakayama, Dr. Akira Koyama, Dr. Chunyu Zhu, Dr. Yoshitaka Aoki, Prof. Hiroki Habazaki*

Division of Applied Chemistry, Faculty of Engineering, Hokkaido University, Sapporo, Hokkaido 060-8628, Japan

habazaki@eng.hokudai.ac.jp

Keywords: Superhydrophobic, superoleophobic, self-healing, hierarchical dual-pore surface, aluminum

This paper reports rapid self-healing on superoleophobic hierarchically porous aluminum surfaces within one hour even at room temperature. This self-healing surface was prepared by infiltration of a liquid fluoroalkylsilane (FAS) coating into the substrate pores. The FAS-infiltrated dual-pore superoleophobic surface becomes superoleophilic after oxygen plasma treatment due to the damage done to the organic coating. However, the superoleophobicity is completely recovered by exposure to normal atmosphere at room temperature, and this rapid self-healing is repeatable. The FAS liquid appears to coat the nanopore walls, rather than filling the nanopores. The high wettability of FAS on surfaces induces the rapid re-coating of the plasma-damaged surface, contributing to the self-healing of the superoleophobicity.

1. Introduction

The surfaces of some plants are superhydrophobic; lotus leaf is one of the well-known examples.[1-2] A superhydrophobic surface is typically defined as a surface that show a water

contact angle higher than 150°, a very low water sliding angle, and/or low contact angle hysteresis (the difference between advancing and receding contact angles). The lotus leaf exhibits self-cleaning properties; in that contaminant particles on its surface are readily removed by rinsing with water droplets.[1] The surface of the lotus leaf consists of nanoscale needle-like wax crystals superimposed on microscale papillae.[1] Such a hierarchically rough surface is crucial for obtaining high water repellency, as well as a surface composition that can reduce surface free energy.

Inspired by nature, many efforts have been made in the last two decades to develop artificial superhydrophobic surfaces on engineering materials for various practical applications,[3-25] such as self-cleaning,[3-9] anti-icing,[10-14] anti-corrosion[15-20] and fluid drag reduction.[21-25] The first artificial superhydrophobic surface was reported in 1996 by Onda *et al*.,[26] who demonstrated a superhydrophobic surface of alkylketendimer (AKD) with fractal surface morphology exhibiting a water contact angle as high as 174°. In 1997, Tadanaga *et al*. fabricated a transparent superhydrophobic coating with nanoscale asperity, formed by boiling water treatment of an alumina thin film prepared by a sol-gel method and subsequent fluoroalkylsilane (FAS) monolayer coating.[27,28] This coating also had superior anti-reflection properties, making it ideal for use as an anti-reflective coating of camera lenses.[29]

Durability of superhydrophobic surfaces is of importance in practical applications. There are two main modes of degradation: physical damage of the highly rough surface geometry and organic contamination of surface from environmental exposure. The latter can be overcome by fabricating a superoleophobic surface. Most solid surfaces are oleophilic, showing static contact angles for low-surface-tension liquids on flat surfaces (< 90°). Surface roughening of the oleophilic surface further reduces the contact angle in accordance with the Wenzel model,[30] but the introduction of special surface geometries such as overhang, re-entrant, hierarchical micro-/nano- dual pillars or dual pore surfaces, together with the

reduction of surface energy, have been utilized to obtain superoleophobic surfaces with contact angles > 150° and contact angle hysteresis < 5° even for low-surface-tension liquids close to 20 mN m^{-1}.[31-39]

Durability is a crucial issue even for superoleophobic surfaces. The authors previously developed a superoleophobic aluminum surface by a combined wet process of chemical etching, anodizing and organic monolayer coating.[40, 41] The obtained hierarchical micro-/nano-dual pore surface with a fluoroalkyl monolayer coating exhibited super-repellency even for liquids with surface tensions as low as ~20 mN m^{-1}. Figure S1 shows the degradation of the superoleophobic aluminum surface by impinging glass beads with diameters of 0.5–0.7 mm and weights of ~0.25 mg (Figure S1a). The advancing contact angles for water and hexadecane remain almost unchanged, but the contact angle hysteresis increases gradually with an increase in impinging cycle (Figure S1b). This surface observation denotes the damage of the monolayer coating, which is obvious from backscattered scanning electron micrographs (composition image) as shown in Figure S1d. After re-coating of the organic monolayer, the surface recovered its superoleophobic character. Thus, the introduction of self-healing functionality to this surface is of crucial interest to obtain durable superoleophobic surfaces.

Self-healing superoleophobic surfaces have been reported recently.[42-52] Zhou *et al.* and Wang *et al.* reported the self-healing superhydrophobic and superoleophobic properties of fabric coatings prepared from a mixture of fluorinated decyl polyhedral oligomeric silsesquioxane and hydrolyzed fluorinated alkylsilane or by an easily available material system consisting of poly(vinylidene fluoride-co-hexafluoropropylene), fluoroalkylsilane, and modified silica nanoparticles. Chemically and mechanically damaged surfaces were restored to their super-liquid repellent states after a brief heat treatment.[42-46] Zhang *et al*. fabricated a self-healing fabric coating with branched thiol-ene fluorinated silixane networks covered with

a fluoroalkylsilane top layer.[47,48] A coating consisting of rod-like palygorskite and organosilanes also revealed self-healing superoleophobicity.[49] Wang *et al*. designed self-healing superoleophobic aluminum by utilizing the nanopores formed after anodizing aluminum as "nanoreservoirs" of healing agent.[46, 50] The superoleophobicity was restored by the transportation/enrichment of low-surface-energy materials trapped in the nanoreservoirs to the outermost surface, which is thermodynamically driven by a minimization of the surface tension. These surfaces, however, require heat treatment at elevated temperatures or long periods of air exposure (>24 h) for self-healing. To the best of our knowledge, there are no examples showing rapid self-healing at ambient temperatures or under normal atmosphere.

Herein, the authors added a liquid healing agent to nanoreservoirs for self-healing of damaged organic coatings on hierarchically rough aluminum surfaces, as schematically illustrated in Figure 1. Self-healing of the degraded superoleophobicity was observed even at room temperature within one hour of beginning the treatment. For fundamental understanding of the healing mechanism as well as the factors influencing the self-healing properties, cylindrical nanopore channels of different diameters and lengths were formed and their self-healing behavior for water repellency was examined.

2. Results and Discussion

2.1. Self-healing superoleophobic surface

The authors recently reported that micro-/nano-dual pore aluminum surfaces produced by chemical etching and anodizing of high purity aluminum show superoleophobicity even for low-surface-tension liquids, such as octane, after fluoroalkylphosphonic acid coating.[40] Figure 2 shows SEM images of the surfaces in this study, where we utilized this hierarchical surface with cylindrical nanopores to add a healing agent into the surface. The morphology of the substrate indicates the micro-/nano-dual porous morphology. Low magnification SEM

images reveal microscale roughness developed by chemical etching. The chemical etching of aluminum in a mixed solution of HCl + $CuCl_2$ forms a number of crystallographic etch pits with a half-cubic morphology as the basic structural unit of each pit.[40, 57] The dissolution of aluminum occurs preferentially in the crystallographic <100> direction,[58, 59] and the size of pits is controlled by the rate of saturation precipitation of $AlCl_3$ that induces passivation of the pits. The small nanopores (Figure 1) were developed by anodization, and the pore size of ~30 nm was controlled by the post pore-widening treatment.

Figure 3 shows the self-healing ability of the superoleophobic dual-pore hierarchical aluminum specimen with infiltrated FAS. The advancing contact angles for both water and hexadecane droplets are higher than 150°, and the values of their contact angle hysteresis are less than 5°; the surface is superoleophobic as reported previously.[40] After oxygen plasma irradiation, the superoleophobic surface becomes superhydrophilic and superoleophilic with an advancing contact angle of ~10°. This is associated with the damage of the fluoroalkyl monolayer by oxygen plasma, as shown in the change in the XPS spectra of the superoleophobic surface without FAP infiltration (Figure S2). The intensity of fluorine is highly reduced after plasma treatment, indicating the removal of the fluoroalkyl layer. For the FAS-infiltrated specimen, the contact angle and contact angle hysteresis were recovered to their original levels (~160° and ~5°, respectively) after air exposure for 1 h at room temperature (Figure 3). The self-healing behavior was also confirmed as shown in Movie S1. A hexadecane droplet (5 μL) was readily rolled off from the original superoleophobic surface, which showed a sliding angle of < 5° (Movie S1a). However, a hexadecane droplet quickly spread over the surface after oxygen plasma irradiation for 120 s due to the degradation of FDPA and FAS at the outermost surface (Movie S1b). After simple air exposure for 1 h, the superoleophobicity with a sliding angle of < 5° was recovered (Movie S1c).

Moreover, this self-healing of the FAS-infiltrated superoleophobic surface is repeatable. We carried out the plasma treatment after each round of 1 h air exposure (Figure 4), and the superhydrophobicity and superoleophobicity were obviously and fully recovered for at least 8 cycles. FAS may suffer from slow hydrolysis in air, but every 24 h of plasma irradiation (Figure S3) exhibits good repeatable superhydrophobicity and superoleophobicity of the FAS-infiltrated hierarchical aluminum surface. The FAS infiltrated into the nanopores and was chemically stable in air, contributing to the repeatable self-healing of the specimen.

2.2. Mechanism of self-healing superoleophobicity

To gain insight into the self-healing mechanism of the FAS-infiltrated hierarchical surface, FAS was infiltrated into simple nanoporous alumina without the designed micro-porous structure, and the healing behavior was examined. Nanoporous alumina films with two different pore sizes were prepared as shown in Figure 5. The size of the smaller nanopores (Figure 5a) is approximately 40 nm, which is similar to that in the hierarchical aluminum specimen described above. The larger nanopores (Figure 5c) have pore sizes of ~120 nm, and the thickness for each porous film with cylindrical morphology is 3 μm (Figure 5b and 5d).

The amount of infiltrated FAS was estimated using GDOES depth profile analysis. Figure 6a shows the elemental depth profiles of the specimen with smaller nanopores before and after FAS infiltration. After FAS infiltration, the intensities of carbon, fluorine and silicone increased throughout the sample, indicating the presence of FAS in the nanopores (Figure 6b). Similar depth profiles were obtained for the specimen with larger nanopores. From the number density of nanopores, as well as the diameter and length of nanopores obtained from SEM observations (Figure 5), the surface area and the pore volume per geometrical area of specimens was roughly estimated (Table 1). The surface area estimated for the smaller-pore specimen is approximately 3.6 times that of the larger one. This value is close to the ratio of the integrated fluorine intensities of GDOES depth profiles for the smaller-pore specimen

relative to those for the larger-pore one before and after FAS infiltration (Table 1). In contrast, the pore volume of the smaller nanopores is similar to that of the larger nanopores. Therefore, the amount of FAS infiltrated into the nanopores is almost proportional to the area of the pore wall surface, not the pore volume. This means that the FAS is likely coating the pore wall, rather than filling the nanopores.

Figure 7 shows the change in wettability of the nanoporous alumina films with and without FAS infiltration before and after plasma treatment. The advancing contact angle for water droplets was approximately 130° on the smaller nanopores with FAS infiltration. This value is similar to that before FAS infiltration, indicating negligible influence of the presence of FAS in the nanopores on the surface wettability. The irradiation of oxygen plasma for 120 s changed the surface to hydrophilic, with contact angles < 10° on all three surfaces. The contact angle on the FAS-free specimen remains almost unchanged during air exposure, whereas recovery of the contact angle proceeds on the FAS-infiltrated specimens. Thus, the FAS is effectively utilized in healing the hydrophobicity and oleophobicity. The recovery of the contact angle is rather rapid, and the steady-state contact angle is obtained within 1 h at room temperature in the air. The recovered angle is dependent upon the size of the nanopores. The specimen with smaller nanopores specimen exhibits a recovered contact angle of ~130°, which is similar to that of the as-received one. In contrast, the contact angle of the specimen with larger nanopores may be related to the damage of FAS in the nanopores due to plasma. GDOES elemental depth profiles of the FAS-infiltrated specimens before and after oxygen plasma irradiation (Figure S4) reveal the decrease fluorine and carbon intensities at the outermost surface after plasma irradiation, contributing to the transition of the surface from hydrophobic to hydrophilic. The intensities of all the elements in the smaller nanopores appear to be unaffected by the plasma. In contrast, the intensities of fluorine and carbon were reduced even in the nanopores when the larger nanopores were irradiated by plasma. The degradation of FAS by plasma in the nanopores suppress the supply of FAS to the outermost

surface, leading to reduced recovery of the contact angle. Thus, the degradation of FAS in nanopores must be avoided to get sufficient self-healing properties.

The influence of the nanopore film thickness on the self-healing behavior was also examined. Figure 8 shows the SEM images of surfaces and cross-sections of porous anodic alumina films formed in sulfuric acid electrolyte for several anodizing times. The thickness of the nanoporous alumina films changes almost linearly with anodizing time from 0.5 μm to 9 μm (Figure 8b to 8f). The nanopores were controlled to a size of ~40 nm by post-pore widening treatment (Figure 8a). Thus, nanoporous alumina films with similar pore structures and different thicknesses were successfully prepared.

Figure 9a shows the effect of nanopore length (porous film thickness) on the self-healing behavior. All the FAS-infiltrated specimens are hydrophobic with contact angles of approximately 130°. Again, oxygen plasma irradiation for 120 s decreased the water contact angle to < 10°, but all the FAS-infiltrated specimens showed self-healing behavior where the water contact angle increased after 1 h. The nanopore length had little influence on the self-healing properties for the specimens with pore lengths of 1.5–9 μm and the contact angles were almost completely recovered to their original value. Only the specimens with a pore length of 0.5 μm showed limited recovery of the contact angle (~110°). The lower amount of FAS present in the shorter nanopores and/or degradation of FAS in the shorter nanopores by plasma may be the roof of this poor self-healing behavior.

The repeatability of self-healing hydrophobicity was also examined (Figure 9b). When the cycle of 1) oxygen plasma irradiation for 120 s and 2) air exposure at room temperature for ~1 h was repeated, all specimens with different pore lengths showed similar recovery of the contact angle to >120°. However, lower recovering contact angles are obtained for the specimens with shorter nanopore lengths at cycles higher than 3. Thus, longer nanopores, which can infiltrate larger amounts of FAS, are preferable for better self-healing durability.

From the findings in this study, we proposed the self-healing process of the superoleophobicity as illustrated in Figure 10. GDOES depth profile analysis suggests that the amount of FAS in the nanopores is approximately proportional to the pore wall surface area, rather than the pore volume. The liquid FAS is, therefore, likely to coat the nanopores (Figure 10a), not to fill the nanopores. As shown in Figure S5a, the static contact angle of an FAS liquid droplets on the flat FDPA coated surface is ~4°. The extremely high wettability of FAS liquid on the FDPA surface may create uniform wetting of the nanopores by FAS. Then, oxygen plasma treatment decomposes the FAS and the FDPA monolayer on the outermost surface (Figure 10b), changing the surface to hydrophilic and oleophilic. The FAS liquid layer on a FDPA monolayer in nanopores will spread again to the outermost surface because of the high wettability on the FDPA surface. Since the plasma-treated aluminum surface shows a static contact angle of ~17° for the FAS liquid (Figure S5b), FAS molecules can gradually spread from the FDPA-coated nanopores over the hydrophilic plasma-damaged outermost surface. Then, the FAS-coated monolayer should be formed on the damaged outermost surface, regenerating the superoleophobic surface (Figure 10c); the superoleophobic state was recovered within 1 h. This rather robust healing may be partly associated with the relatively small interpore distances of 15–20 nm.

Healing via a vapor phase is another possible route, but the vapor pressure of FAS is not high enough at room temperature (< 0.1 Pa) for this to function in our systems. In addition, rather long self-healing durability (Figure S3) suggests that the loss of FAS by evaporation may be limited at room temperature. In other words, further rapid self-healing could be achieved at elevated temperatures, although maintaining the healing durability the reserved amount of FAS liquid needs to be increased by further controlling the pore morphology. The use of liquid healing agent with high wettability for the pore wall surface is likely suitable for room-temperature self-healing of surface superoleophobicity.

3. Conclusions

This study demonstrated the room-temperature self-healing of superoleophobic hierarchically porous aluminum surfaces with infiltrated FAS liquid. The FAS-infiltrated superoleophobic surface became superhydrophilic and superoleophilic after oxygen plasma irradiation, but self-healed to a superhydrophobic and superoleophobic state after 1 h exposure to normal atmosphere at room temperature. The FAS was liquid at room temperature and appeared to coat the nanopores that were formed by anodizing of aluminum, rather than filling them. The FDPA monolayer-coated surface showed high wettability for FAS liquid, so that the hydrophilic and oleophilic outermost surface formed by oxygen plasma was healed by spreading the FAS liquid from nanopores to the damaged outermost surface. The FAS monolayer coated outermost surface was then regenerated, recovering the high contact angles for both water and hexadecane (> 150°) without any heat treatment. The formation of longer nanopore channels was preferable for improving the durability of such surfaces, since a higher amount of FAS liquid was stored in the nanopores.

4. Experimental section

4.1. Formation of nanoporous surfaces

High-purity aluminum plate (99.999% purity) 0.5 mm in thickness was used in this study as a substrate. The aluminum plate was first electropolished in a solution containing perchloric acid and ethanol (1:4, v/v) at a constant voltage of 20 V for 5 min below 278 K. Then, nanoporous alumina films were formed by anodizing in 0.3 M sulfuric or phosphoric acids at a constant voltage of 25 or 120 V respectively at 288 K for various periods of time to form variable nanoporous alumina films. The nanopore diameter increased with the anodizing voltage regardless of the acid electrolyte used.[53, 54] As the suitable anodizing voltage range is dependent upon the electrolyte,[55, 56] two different acid electrolytes were used in this study.

4.2. Formation of dual-pore hierarchically rough surfaces

Hierarchical dual-pore surfaces were prepared by a combination of chemical etching and anodizing of high purity aluminum. Prior to chemical etching, the aluminum plate was pre-

treated in 1 M sodium hydroxide solution at 333 K for 120 s and subsequently in 1 M nitric acid at 333 K for 180 s to remove the native oxide layer. Chemical etching was carried out by immersing the plate in a mixed solution of 0.2 M $CuCl_2$ and 1 M HCl at 298 K for 360 s. After chemical etching, the specimen was rinsed with concentrated nitric acid to remove the copper deposited on the surface. Then, the etched aluminum specimen was anodized in 0.3 M sulfuric acid at a constant voltage of 25 V for 1200 s at 288 K. Subsequently, the size of the nanopores in the anodic alumina layer was controlled by subsequent pore widening treatment in 5 wt% phosphoric acid at 303 K for 1200 s.

4.3. Organic monolayer coating and infiltration of low-surface-tension molecules in nanopores

An organic self-assembled monolayer was coated on the specimens by immersion in ethanol containing 1 mM 1H,1H,2H,2H-perfluorodecylphosphonic acid ($CF_3(CF_2)_7(CH_2)_2PO(OH)_2$, FDPA) for 24–48 h at room temperature after cleaning the anodized specimens using a plasma cleaner (Harrick Plasma Co., PDC-32G), by which a contaminant hydrocarbon layer was removed from the surfaces. Specimens were then immersed in hexane containing 20 vol% 1H,1H,2H,2H-perfluorodecyltriethoxysilane ($CF_3(CF_2)_7(CH_2)_2Si(OCH_2CH_3)_3$, FAS) for 60 s at room temperature to infiltrate the low-surface-tension molecules (healing agent). The FAS is liquid at room temperature.

4.4. Characterization

Before and after infiltration of FAS, elemental depth profile analysis of the specimens was performed by grow-discharge optical emission spectroscopy (GDOES) using a Jobin Yvon 5000 RF instrument in a neon atmosphere of 1100 Pa by applying a power of 35 W. Light emissions at the characteristic wavelength were monitored throughout the analysis with a sampling time of 0.01 s to obtain a depth profile. The wavelengths of the spectral lines used here were 121.567 nm for hydrogen, 165.705 nm for carbon, 130.217 nm for oxygen, 685.601

nm for fluorine, 396.152 nm for aluminum, 178.287 nm for phosphorus, and 288.115 nm for silicone. The signals were detected from a circular area approximately 4 mm in diameter. The morphological images were taken using a JEOL, JSM-6500F field emission scanning electron microscope (FE-SEM) operated at 10 kV. The surface of some specimens was also examined by a JEOL, JPS-9200 X-ray photoelectron spectroscopy (XPS) with Mg Kα excitation (hν = 1253.6 eV). The binding energy of each species were calibrated using a contaminant hydrocarbon peak (285.0 eV). The spectra were obtained without any Ar ion etching in the XPS chamber.

4.5. Wettability evaluations

Surface wettability was evaluated by static and dynamic contact angle measurements for water (surface tension of 73 $mN \cdot m^{-1}$) and hexadecane (28 $mN \cdot m^{-1}$) droplets (4 μL) using an optical contact angle meter (Kyowa Interface Science Co., DM-CE1). Dynamic contact angle measurements were performed using an expansion/contraction method.[27] Self-healing properties were evaluated by static and dynamic contact angle measurements immediately after irradiation of oxygen plasma for 120 s, and also after subsequent air exposure in atmosphere at room temperature for a suitable period of time (1–8 h).

Supporting Information

Supporting Information is available from the Wiley Online Library or from the author.

Acknowledgements

This work was supported in part by JSPS KAKENHI Grant Number 15J00802 and the Light Metal Educational Foundation.

Received: ((will be filled in by the editorial staff))
Revised: ((will be filled in by the editorial staff))
Published online: ((will be filled in by the editorial staff))

References

[1] W. Barthlott, C. Neinhuis, *Planta* **1997**, 202, 1-8.

[2] J. T. Simpson, S. R. Hunter, T. Aytug, *Rep. Prog. Phys.* **2015**, 78, 086501.

[3] R. Blossey, *Nat. Mater.* **2003**, 2, 301-306.

[4] R. Fürstner, W. Barthlott, *Langmuir* **2005**, 21, 956-961.

[5] O. U. Nimittrakoolchai, S. Supothina, *J. Eur. Ceram. Soc.* **2008**, 28, 947-952.

[6] B. Bhushan, Y. C. Jung, K. Koch, *Langmuir* **2009**, 25, 3240-3248.

[7] I. Sas, R. E. Gorga, J. A. Joines, K. A. Thoney, *J. Polym. Sci. B* **2012**, 50, 824-825.

[8] G. Zhou, J. He, L. Gao, T. Ren, T. Li, *RSC Adv.* **2013**, 3, 21789-21796.

[9] C. Xue, X. Guo, J. Ma, S. Jia, *ACS Appl. Mater. Interfaces* **2015**, 7, 8251-8259.

[10] L. Cao, A. K. Jones, V. K. Sikka, J. Wu, D. Gao, *Langmuir* **2009**, 25, 12444-12448.

[11] S. Farhadi, M. Farzaneh, S. A. Kulinich, *Appl. Surf. Sci.* **2011**, 257, 6264-6259.

[12] P. Guo, Y. Zheng, M. Wen, C. Song, Y. Lin, L. Jiang, *Adv. Mater.* **2012**, 24, 2642-2648.

[13] Y. Wang, J. Xue, Q. Wang, Q. Chen, J. Ding, *ACS Appl. Mater. Interfaces* **2013**, 5, 3370-3381.

[14] J. Lv, Y. Song, J. Wang, *ACS Nano* **2014**, 8, 3152-3169.

[15] K. Liu, M. Zhang, J. Zhai, J. Wang, L. Jiang, *Appl. Phys. Lett.* **2008**, 92, 183103.

[16] W. Xu, J. Song, J. Sun, Y. Lu, Z. Yu, *ACS Appl. Mater. Interfaces* **2011**, 3, 4404-4414.

[17] N. Valipour Motlagh, F. C. Birjandi, J. Sargolzaei, N. Shahtahmassebi, *Appl. Surf. Sci.* **2013**, 283, 636-647.

[18] M. F. Montemor, *Surf. Coat. Technol.* **2014**, 258, 17-37.

[19] S. Esmailzadeh, S. Khorsand, K. Raeissi, F. Ashrafizadeh, *Surf. Coat. Technol.* **2015**, 283, 337-346.

[20] S. Zheng, C. Li, Q. Fu, M. Li, W. Hu, Q. Wang, M. Du, X. Liu, Z. Chen, *Surf. Coat. Technol.* **2015**, 276, 341-348.

[21] D. Zhang, L. Wang, H. Qian, X. Li, *J. Coat. Technol. Res.* **2016**, 13, 11-29.

[22] K. Fukagata, N. Kasagi, P. Koumoutsakos, *Phys. Fluids* **2006**, 18, 051703.

[23] N. J. Shirtcliffe, G. McHale, M. I. Newton, Y. Zhang, *ACS Appl. Mater. Interfaces* **2009**, 1, 1316-1323.

[24] S. Srinivasan, J. A. Kleingartner, J. B. Gilbert, R. E. Cohen, *Phys. Rev. Lett.* **2015**, 114, 014501.

[25] K. M. Tanvir Ahmmed, A. M. Kietzig, *Soft Matter* **2016**, 12, 4912-4922.

[26] T. Onda, S. Shibuichi, N. Satoh, K. Tsujii, *Langmuir* **1996**, 12, 2125-2127.

[27] K. Tadanaga, N. Katata, T. Minami, *J. Am. Ceram. Soc.* **1997**, 80, 1040-1042.

[28] K. Tadanaga, N. Katata, T. Minami, *J. Am. Ceram. Soc.* **1997**, 80, 3213-3216.

[29] K. Tadanaga, *J. Ceram. Soc. Jpn.* **2013**, 121, 819-824.

[30] R. N. Wenzel, *Ind. Eng. Chem.* **1936**, 28, 988-994.

[31] A. Tuteja, W. Choi, M. Ma, J. M. Mabry, S. A. Mazzella, G. C. Rutledge, G. H. McKinley, R. E. Cohen, *Science* **2007**, 318, 1618-1622.

[32] A. Tuteja, W. Choi, J. M. Mabry, G. H. McKinley, R. E. Cohen, *Proc. Natl. Acad. U.S.A.* **2008**, 105, 18200-18205.

[33] T. Fujii, Y. Aoki, H. Habazaki, *Langmuir* **2011**, 27, 11752-11756.

[34] T. Fujii, H. Sato, E. Tsuji, Y. Aoki, H. Habazaki, *J. Phys. Chem. C* **2012**, 116, 23308-23314.

[35] H. Zhao, K. Park, K. Law, *Langmuir* **2012**, 28, 14925-14934.

[36] T. Jiang, Z. Guo, W. Liu, *J. Mater. Chem. A* **2015**, 3, 1811-1827.

[37] M. Kuang, J. Wang, L. Jiang, *Chem. Soc. Rev.* **2016**, 45, 6833-6854.

[38] Z. Wang, M. Elimelech, S. Lin, *Environ. Sci. Technol.* **2016**, 50, 2132-2150.

[39] J. Yong, F. Chen, Q. Yang, J. Huo, X. Hou, *Chem. Soc. Rev.* **2017**, 46, 4168-4217.

[40] K. Nakayama, E. Tsuji, Y. Aoki, H. Habazaki, *RSC Adv.* **2014**, 4, 30927-30933.

[41] K. Nakayama, E. Tsuji, Y. Aoki, S. G. Park, H. Habazaki, *J. Phys. Chem. C* **2016**, 120, 15684-15690.

[42] H. Wang, Y. Xue, J. Ding, L. Feng, X. Wang, T. Lin, *Angew. Chem. Int. Ed.* **2011**, 50, 11433-11436.

[43] H. Wang, H. Zhou, A. Gestos, J. Fang, T. Lin, *ACS Appl. Mater. Interfaces* **2013**, 5, 10221-10226.

[44] H. Zhou, H. Wang, H. Niu, A. Gestos, T. Lin, *Adv. Funct. Mater.* **2013**, 23, 1664-1670.

[45] H. Zhou, H. Wang, H. Niu, Y. Zhao, Z. Xu, T. Lin, *Adv. Funct. Mater.* **2017**, 27, 1604261.

[46] K. Chen, Y. Wu. S. Zhou, L. Wu, *Macromol. Rapid Commun.* **2016**, 37, 463-485.

[47] H. Zhang, J. J. Tan, Y. Liu, C. P. Hou, *Mater. Des.* **2017**, 135, 16-25.

[48] H. Zhang, Y. Liu, C. Hou, Y. Ma, *Surf. Coat. Technol.* **2017**, 331, 97-106.

[49] B. Li, J. Zhang, *Chem. Commun.* **2016**, 52, 2744-2747.

[50] X. Wang, X. Liu, F. Zhou, W. Liu, *Chem. Commun.* **2011**, 47, 2324-2326.

[51] K. Ellinas, A. Tserepi, E. Gogolides, *Adv. Colloid Interface Sci.* **2017**, 250, 132-157.

[52] K. Golovin, M. Boban, J. M. Mabry, A. Tuteja, *ACS Appl. Mater. Interfaces* **2017**, 9, 11212-11223.

[53] S. Ono, *J. Vac. Soc. Jpn.* **2009**, 52, 637-644.

[54] W. Lee, S. J. Park, *Chem. Rev.* **2014**, 114, 7487-7556.

[55] S. Ono, M. Saito, M. Ishiguro, H. Asoh, *J. Electrochem. Soc.* **2004**, 151, B473-B478.

[56] B. Gastón-García, E. García-Lecina, J. A. Díez, M. Belenguer, C. Müller, *Electrochem. Solid-State Lett.* **2010**, 13, C33-C35.

[57] D. Wang, L. Zang, W. Lee, M. Knez, L. Liu, *Small* **2013**, 9, 1025-1029.

[58] C. K. Dyer, R. S. Alwitt, *J. Electrochem. Soc.* **1981**, 128, 300-305.

[59] S. Ono, H. Habazaki, *Corros. Sci.* **2009**, 51, 2364-2370.

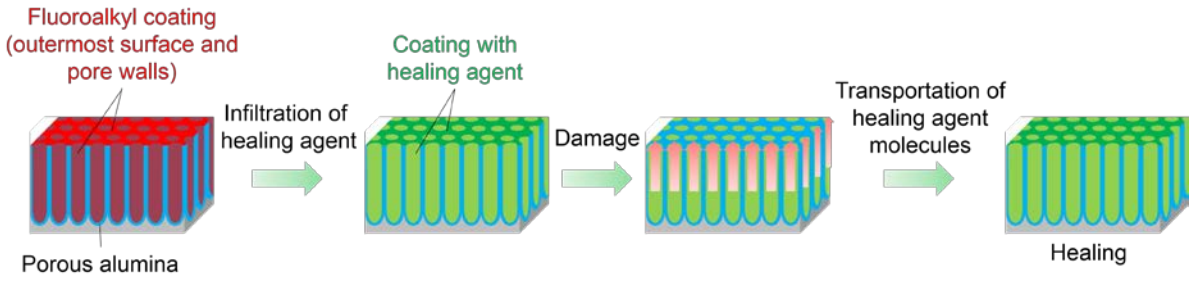

Figure 1. Schematic illustration showing self-healing by infiltration of low-surface-energy material into anodic nanopores.

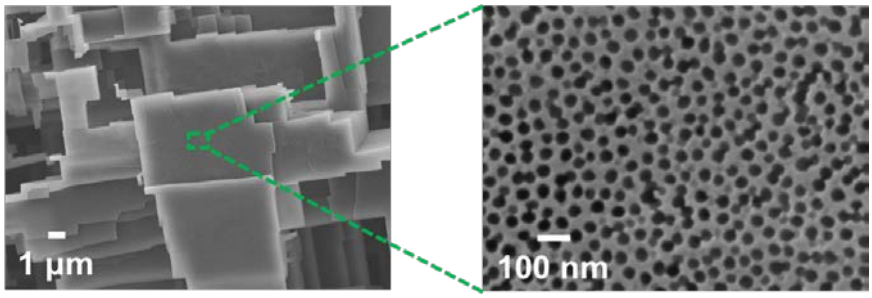

Figure 2. SEM images of the hierarchically rough aluminum surface chemically etched in solution containing 0.2 M $CuCl_2$ and 1 M HCl for 360 s and then anodized in 0.3 M sulfuric acid electrolyte at a constant voltage of 25 V for 20 min at 288 K, followed by pore-widening in 5 wt% phosphoric acid for 20 min at 303 K.

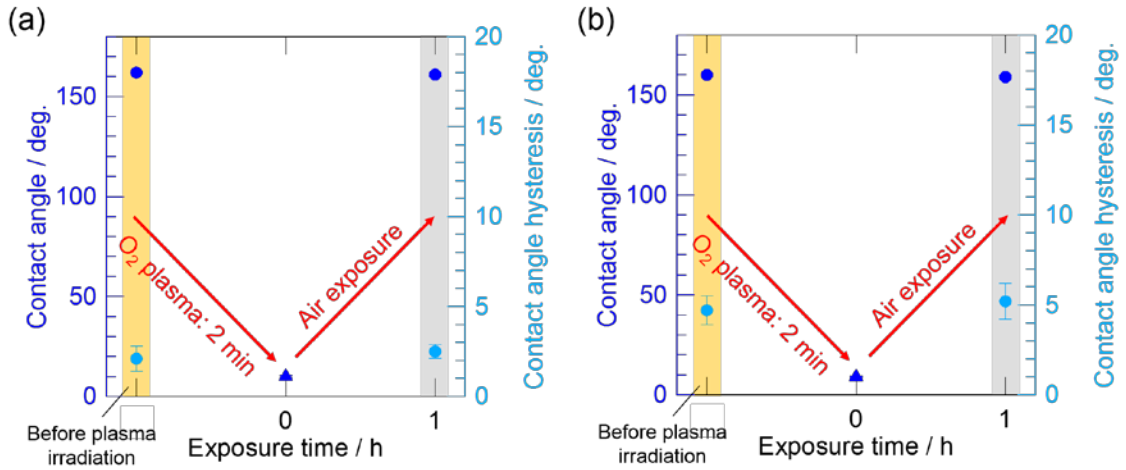

Figure 3. Self-healing behavior on superoleophobic dual-pore hierarchically rough aluminum surfaces for (a) water and (b) hexadecane. Red circles and triangles are advancing and static contact angles, respectively.

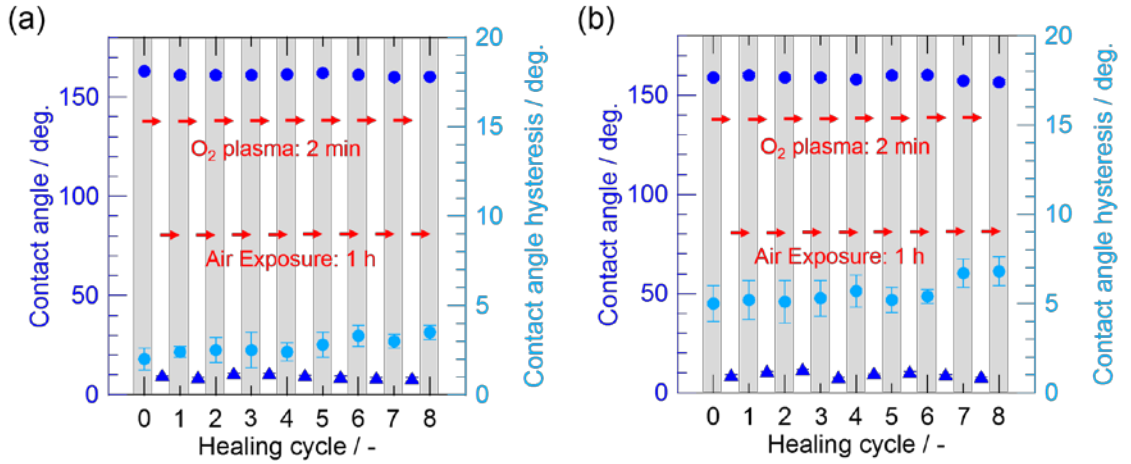

Figure 4. Repeated self-healing properties by hourly plasma irradiation on the FAS-infiltrated hierarchically rough aluminum surface: (a) water and (b) hexadecane droplets.

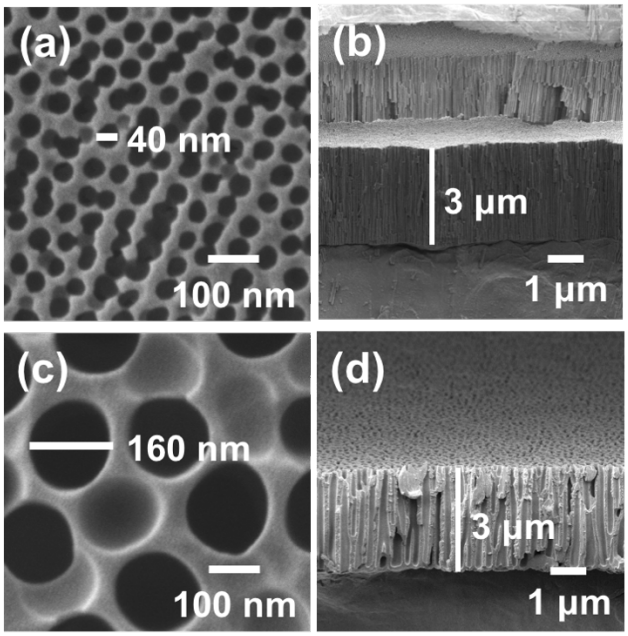

Figure 5. (a, c) Surface and (b, d) cross-sectional SEM images of porous anodic alumina films formed in 0.3 M (a, c) sulfuric acid or (b, d) phosphoric acid at a constant voltage of 25 or 120 V for 20 or 60 min at 288 K and then pore-widened in 5 wt% phosphoric acid for 20 or 60 min at 303 K, respectively.

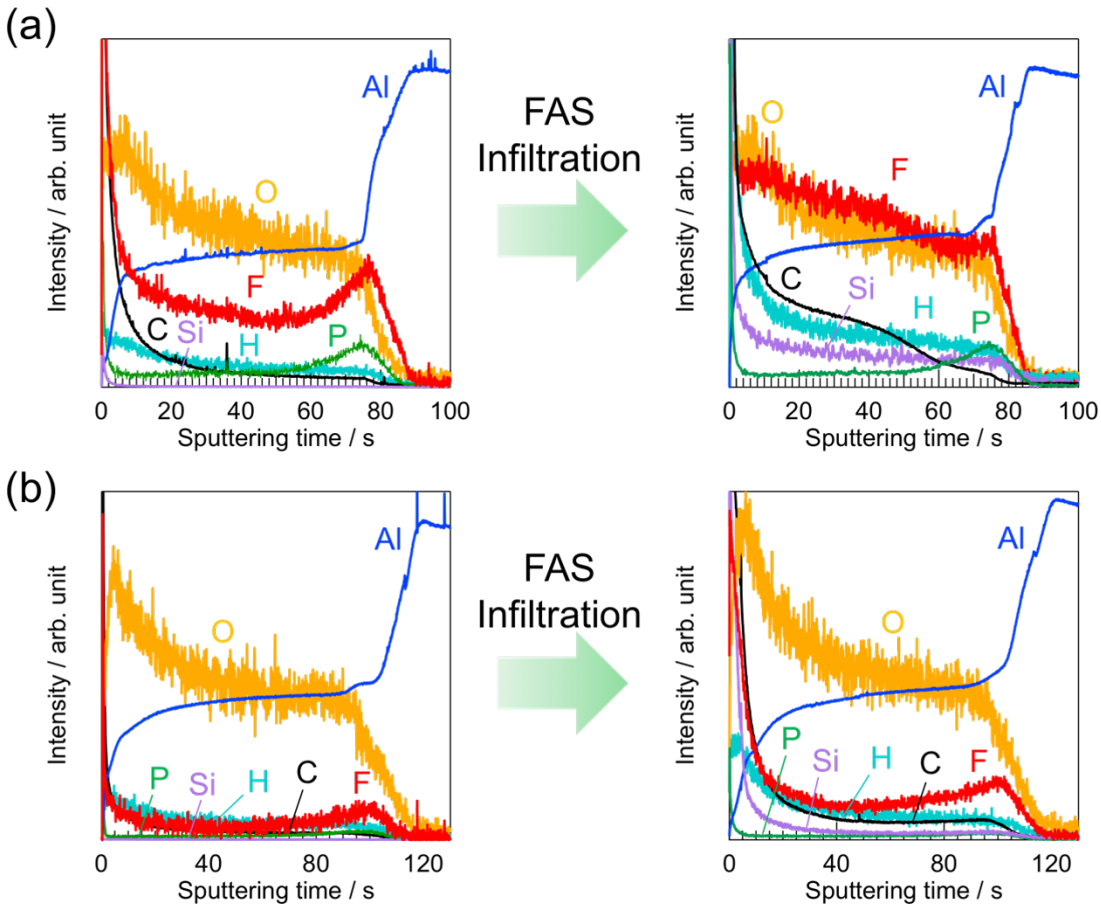

Figure 6. GDOES elemental depth profiles before and after FAS infiltration for porous alumina with (a) smaller and (b) larger nanopores.

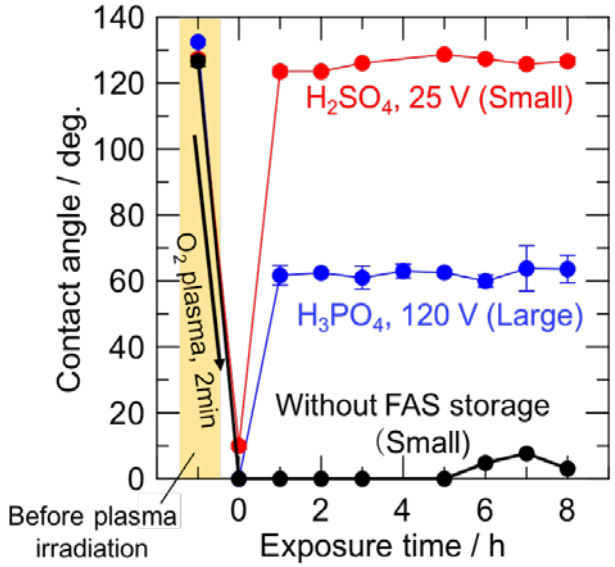

Figure 7. Self-healing behavior on porous alumina surfaces with smaller and larger nanopores with and without infiltrated FAS.

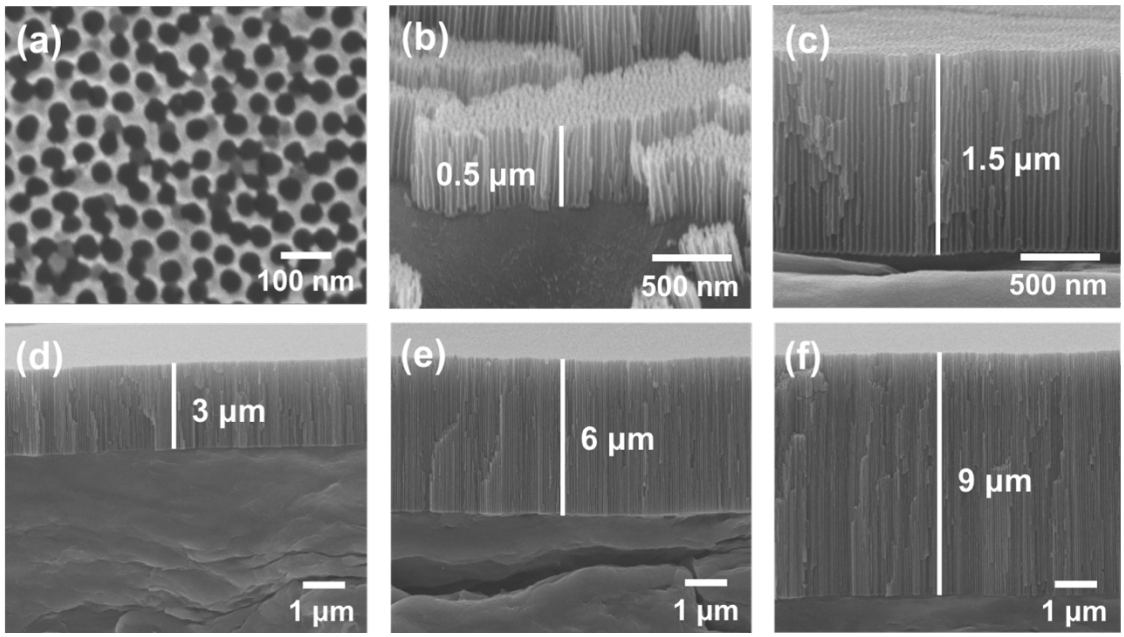

Figure 8. (a) Surface and (b-f) cross-sectional SEM images of porous alumina films formed by anodizing in 0.3 M sulfuric acid electrolyte at a constant. voltage of 25 V for (b) 3, (c) 10, (d) 20, (e) 40 and (f) 60 min at 288 K and then pore-widened in 5 wt% phosphoric acid for 20 min at 303 K. The image of (a) shows the surface of (c).

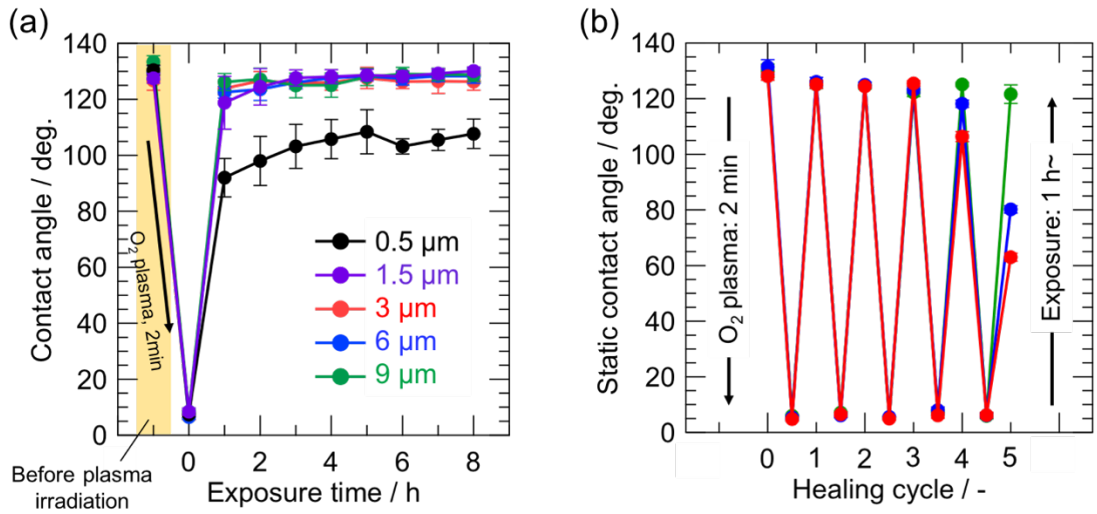

Figure 9. Dependence of nanopore length on (a) self-healing behavior with air exposure for 1-8 h and (b) repeatability of self-healing on porous alumina specimens formed in 0.3 M sulfuric acid electrolyte at a constant voltage of 25 V for (red) 20, (blue) 40 and (green) 60 min at 288 K and then pore-widened in 5 wt% phosphoric acid for 20 min at 303 K.

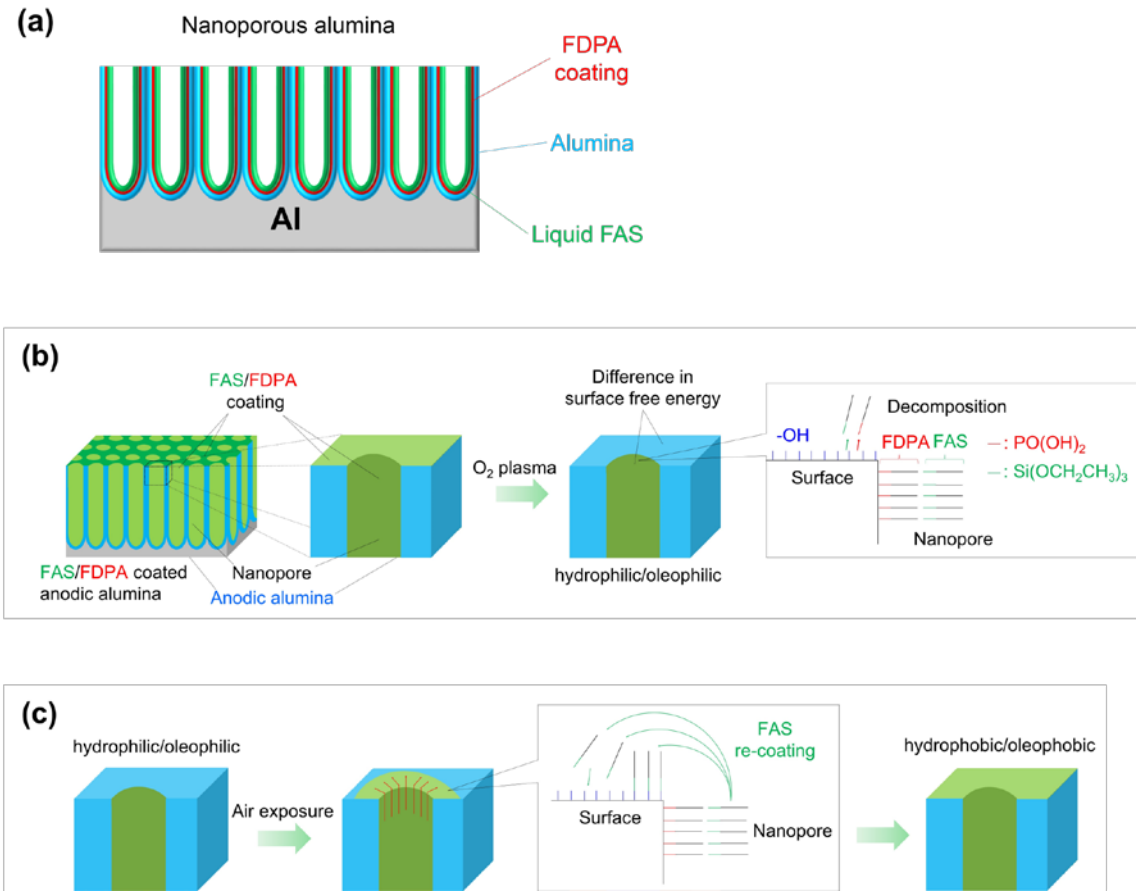

Figure 10. Schematic illustration showing the self-healing in this study using FAS-infiltrated porous surfaces with (a) small or (b) large nanopores, and (c) self-healing mechanism.

Table 1. Pore volume and surface area per geometrical area of specimen and GDOES relative fluoride intensity before and after FAS infiltration

	Pore volume (10^{17} nm^3 cm^{-2})	Surface area (10^{16} nm^2 cm^{-2})	GDOES relative fluorine intensity	
			Before FAS infiltration	After FAS infiltration
Smaller pore	1.4	1.4	3.3	3.6
Larger pore	1.5	0.39	1	1

TOC

Rapid and repeatable self-healing of superoleophobic surfaces is fabricated in this study by infiltration of fluoroalkylsilane liquid, which acts as a healing agent of organic monolayer coating, in nanopore channels of hierarchical mico-/nano-pore surface. The hierarchical porous structure is developed by industrially applicable chemical etching and anodizing of aluminum metal.

Keyword

Superhydrophobic, superoleophobic, self-healing, hierarchical dual-pore surface, aluminum

Katsutoshi Nakayama*, Akira Koyama, Chunyu Zhu, Yoshitaka Aoki, Hiroki Habazaki

Rapid and Repeatable Self-Healing Superoleophobic Porous Aluminum Surface Using Infiltrated Liquid Healing Agent

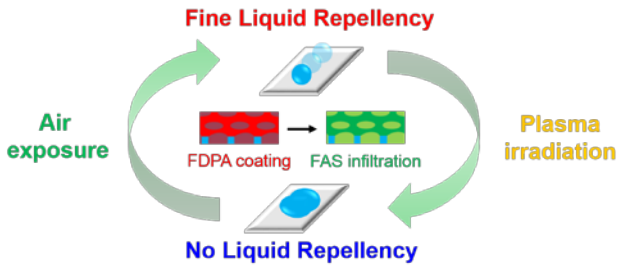

Supporting Information

Rapid and Repeatable Self-Healing Superoleophobic Porous Aluminum Surface Using Infiltrated Liquid Healing Agent

Katsutoshi Nakayama, Akira Koyama, Chunyu Zhu, Yoshitaka Aoki, Hiroki Habazaki**

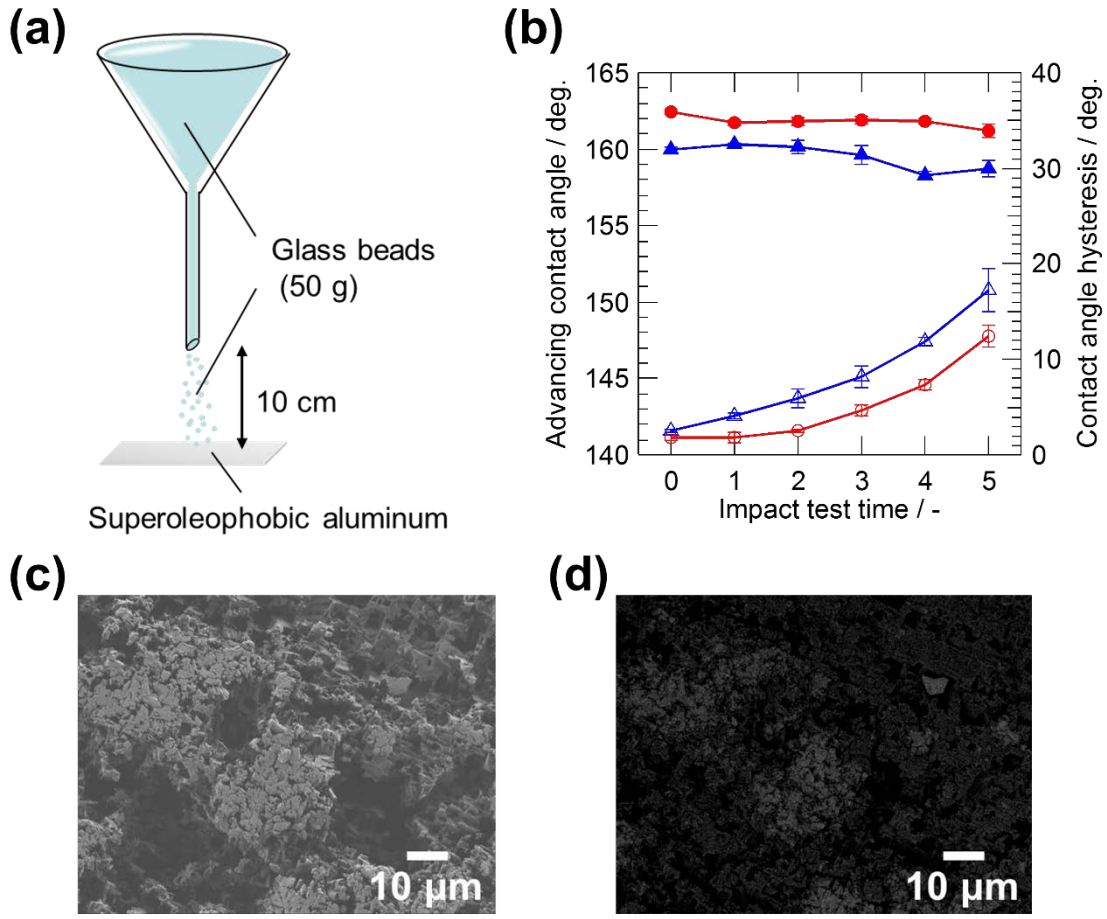

Figure S1. (a) Schematic illustration showing dropping of glass beads 0.5–0.7 mm in diameter and weighing ~0.25 mg from a height of 10 cm. (b) The change in the dynamic contact angles for water and hexadecane as a function of dropped number of glass beads (50 g and ~20,000 beads per cycle). (c, d) Second electron and back-scattered SEM images of after dropping beads (50 g) 5 times, respectively.

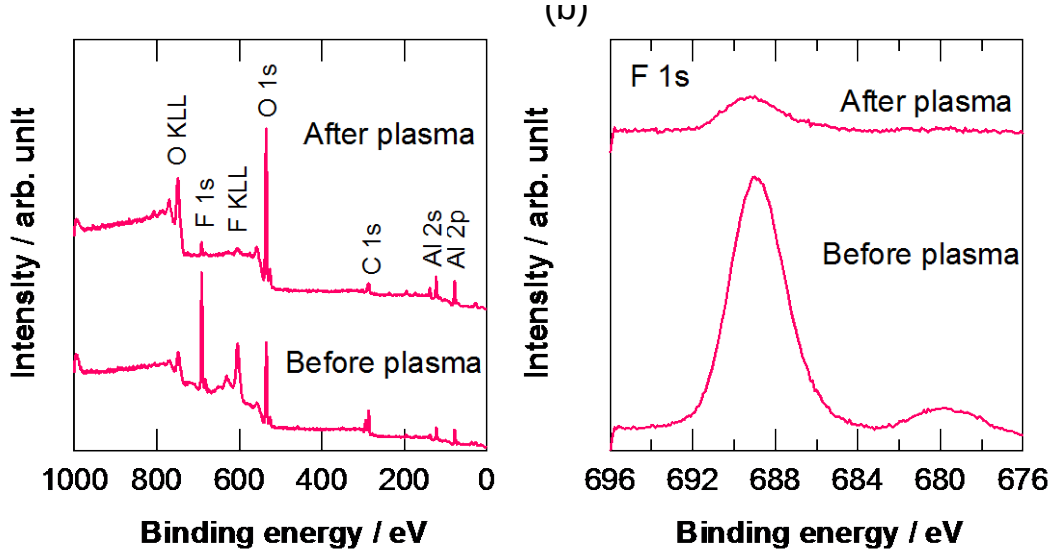

Figure S2. XPS (a) wide scan and (b) F 1s spectra of hierarchically rough superoleophobic aluminum surface without FAS infiltration before and after plasma irradiation.

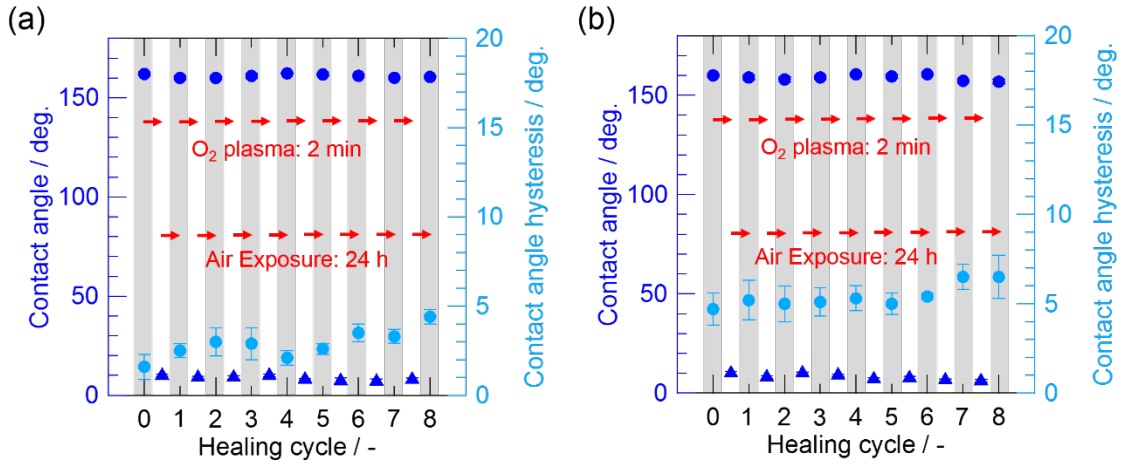

Figure S3. Repeated self-healing by plasma irradiation every 24 h on the FAS-infiltrated hierarchically rough aluminum surface: (a) water and (b) hexadecane droplets.

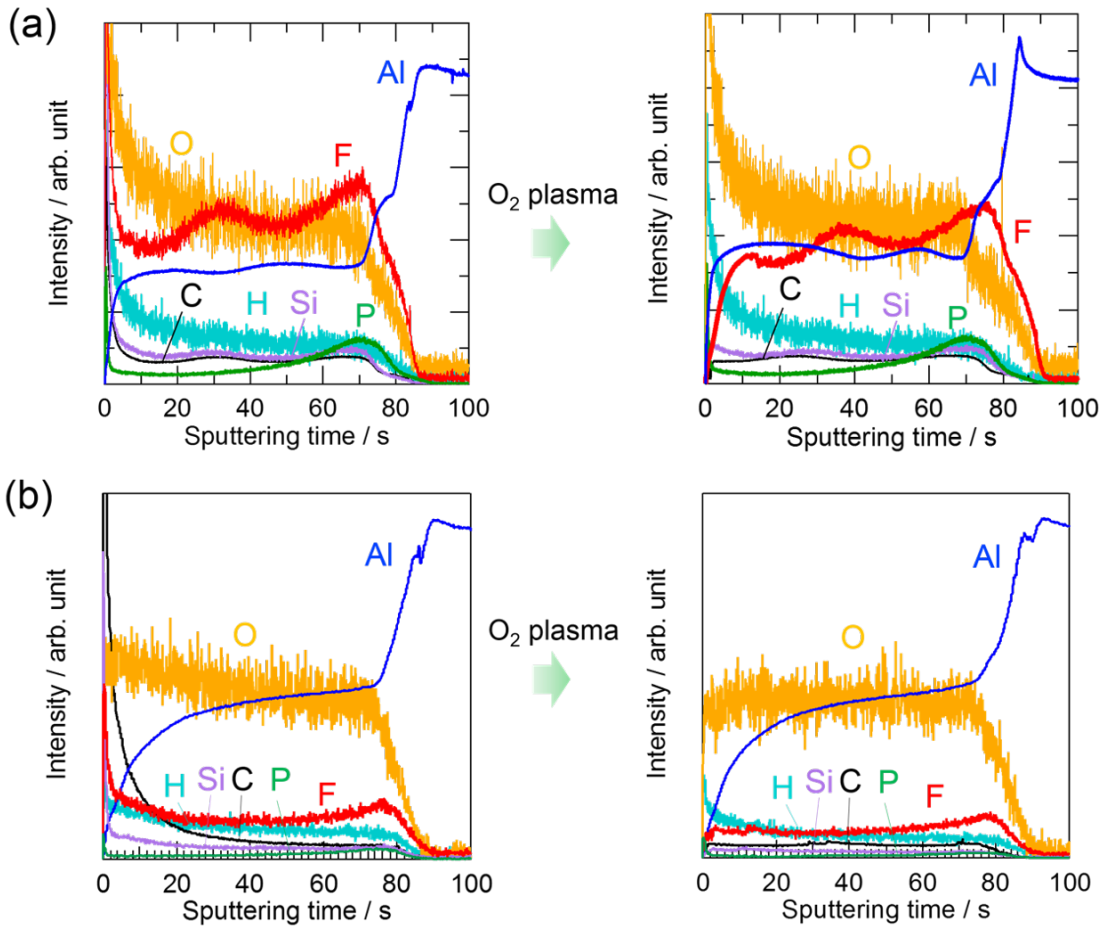

Figure S4. GDOES elemental depth profiles of porous alumina specimens with (a) small and (b) large nanopores with FAS infiltration before and after oxygen plasma irradiation for 120 s.

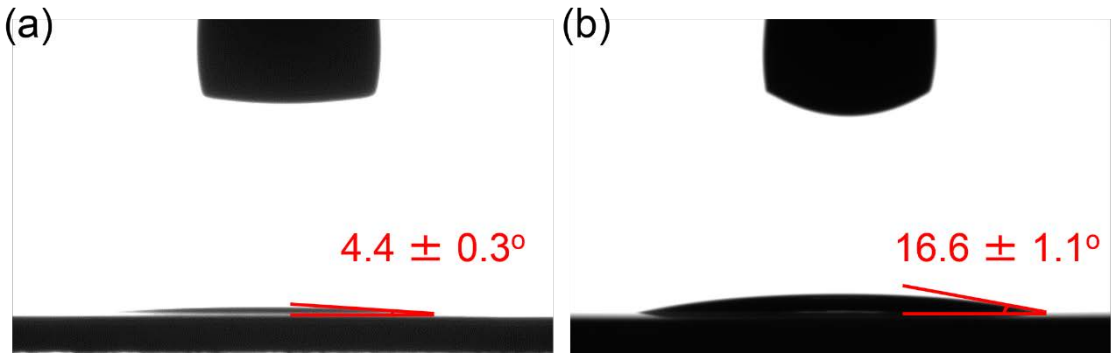

Figure S5. Digital photographs and contact angles of FAS droplets on the flat aluminum surfaces (a) with FDPA coating and (b) immediately after O_2 plasma treatment without FDPA coating.

Movie S1. The sliding behavior of hexadecane droplets (5 μL) on (a) the super-liquid-repellent aluminum surface with FDPA coating and FAS infiltration, (b) after oxygen irradiation for 120 s and (c) after air exposure for >1 h.